

# Coherence and polarization of light propagating through scattering media and biological tissues

Gilbert Jarry, Elisa Steimer, Vivien Damaschini, Michael Epifanie, Marc Jurczak, and Robin Kaiser

The degree of polarization of light propagating through scattering media was measured as a function of the sample thickness in a Mach-Zehnder interferometer at a wavelength of  $\lambda = 633$  nm. For polystyrene microspheres of diameters 200, 430, and 940 nm, depolarization began to appear for thicknesses larger than 23, 19, and 15 scattering mean free paths (SMFP's), respectively, where the coherently detected scattered component dominates the ballistic component. For large particles (940 nm) the initial polarization survived partially in the scattering regime and progressively vanished up to the detection limit of our setup. This phenomenon was similarly observed in diluted blood from 12.5 to 280 SMFP's. Beyond this thickness the fluctuating parallel and crossed components of polarization became random. A dual-channel interferometer allowed us to detect simultaneously the low-frequency fluctuations of both polarized components through a few millimeters in liver tissue. © 1998 Optical Society of America

OCIS codes: 040.2840, 170.3660, 170.4580, 260.5430.

## 1. Introduction

For medical applications such as optical tomography and spectroscopic measurements it is useful to know the maximum tissue depth that can be investigated with collimated light by use of pure spatial discrimination techniques. There are various methods for selecting straightforward transmitted light in tissue: geometrical collimation,<sup>1-3</sup> time-resolved detection,<sup>4-6</sup> correlation of time gating with degenerate four-wave mixing,<sup>7</sup> and low-coherence interferometry.<sup>8-10</sup> The best results for imaging of tissue as much as 1 mm in depth were obtained by a combination of methods, namely, by use of spatial collimation and low-coherence interferometry with femtosecond pulses.<sup>11-13</sup> Moreover, the possibility of using the polarization of transmitted light for imaging tissues has been mentioned<sup>2</sup>; recently more-extensive stud-

ies have been reported that aim at improving the spatial resolution by selecting the polarization of detected light for particle suspensions.<sup>14-16</sup> Coherent methods detect light matched with a reference beam. Consequently, scattered photons that have lost their initial straightforward direction, temporal coherence, or polarization should not be detected. Despite the use of the interferometric low-coherence technique, some scattered light may be coherently detected in systems for tomography, leading to image degradation.<sup>17-19</sup> The preservation of light polarization has also been considered as an indication for forward, on-axis light propagation. Such investigations have been performed with lock-in detection,<sup>14-16</sup> spatial selection,<sup>20</sup> or time-resolved detection schemes.<sup>15</sup> In a recent polarization study of time-resolved transmission of light through suspensions of polystyrene beads it was reported that the snake component, which arrives immediately after the ballistic component, is still partially polarized.<sup>21</sup>

The current challenge in optical tomography consists in achieving metabolic images through parts of the human body. One possibility for doing this is to use spectroscopic changes in tissue that are related to its metabolic level, which provides useful information in both physiological and pathological conditions.<sup>22-24</sup> Unfortunately, purely collimated or ballistic photons disappear after a few hundred micrometers.<sup>18,25</sup> Therefore to investigate thick tissues one must extract information from scattered light. Despite the

---

G. Jarry (gjarry@clubinternet.fr), E. Steimer, V. Damaschini, M. Epifanie, and M. Jurczak are with Laboratoire de Physique des Lasers, Centre National de la Recherche Scientifique, Unité Mixte de Recherche 7538, 93430 Villetaneuse, and Service de Cardiologie, Hôpital d'Instruction des Armées du Val de Grâce, 75230 Paris Cedex 05, France. R. Kaiser is with Institut Non Linéaire de Nice, Centre National de la Recherche Scientifique, Unité Mixte de Recherche 6618, 1361, Route des Lucioles, 06560 Valbonne, France.

Received 5 June 1998; revised manuscript received 27 July 1998.  
0003-6935/98/317357-11\$15.00/0

© 1998 Optical Society of America

appearance a few publications based on the filtering of transmitted photons in the Fourier plane,<sup>26,27</sup> frequency-domain diffusing-photon tomography,<sup>26</sup> and/or axial tomography,<sup>29</sup> the use of snake photons as a diagnostic has not been extensively studied. On the one hand, snake photons contribute to noise or image degradation in low-coherence interferometry because they can be coherently detected.<sup>17–19</sup> On the other hand, however, they can be useful for imaging tissues with a thickness exceeding the maximum path length that photons can pass through in a ballistic regime.<sup>29</sup>

Multiple scattering of light from particles in highly scattering media randomizes the direction of propagation and the state of polarization. However, the polarization memory effect that has been observed over distances much larger than the domain of the ballistic regime<sup>30–32</sup> suggests that some information about the polarization of the incident light is not lost in the scattering regime of propagation. Finally, light propagating in a dense biological tissue becomes depolarized, but one knows little about the spatial scale of this phenomenon. In understanding how light propagates through tissues, another important question to answer concerns the nature of intracellular or tissular components that interact with light at a given wavelength and lead to scattering and depolarization. Most of the theoretical studies on multiple light scattering have considered linear, isotropic, homogeneous, nonabsorbing media made of noninteracting particles. Mammalian tissues are quite different from such models. However, only a few papers have been devoted to the forward propagation of light (transillumination) that can be applied in medicine to investigate thick samples.

For studying the polarization evolution in highly scattering media, radiative transfer equations have been obtained for linearly and circularly polarized incident light.<sup>33</sup> More recently, Bicout *et al.* developed a numerical simulation to study the depolarization of multiple-scattering light as a function of the number of scattering events through suspensions that obey the Rayleigh, intermediate, or Mie scattering regimes.<sup>30,34</sup> Their model, verified by experimental measurements performed with latex beads in water, clearly shows the influence of the particle size on the characteristic length of depolarization.

By measuring the transmitted light through polystyrene bead suspensions and blood samples with heterodyne detection, we previously studied the scattered component of the transmitted light.<sup>35</sup> That is, we underlined the role played by the diameter of the scattering particles on the threshold at which the scattered component dominates the collimated component. Above this threshold, the scattered component was also observed by a coherent off-axis detection method.

In this paper we present additional experiments that address the relation between the loss of coherence and depolarization through polystyrene suspensions, mammalian blood, and liver tissue samples. We have investigated the degree of polarization of the

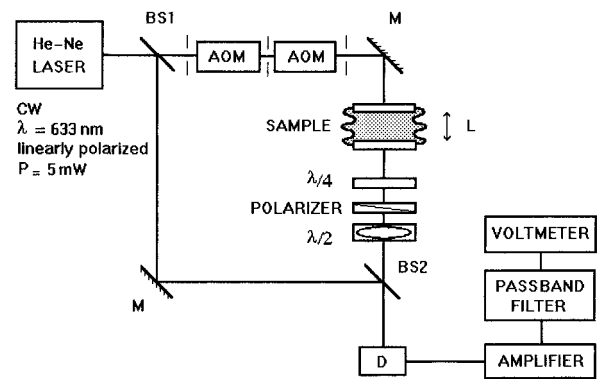


Fig. 1. Schematic diagram of the experimental setup. Polarizing components and retarding plates can be inserted according to the chosen polarization state.  $\lambda/2$ , half-wave plate;  $\lambda/4$ , quarter-wave plate; AOM's, acousto-optic modulators; D, P-I-N diode detector; L, adjustable path length; M's, mirrors; BS1, BS2, beam splitters.

transmitted light in a coherent detection scheme as a function of sample thickness for polystyrene microsphere suspensions and blood dilutions. Identical experiments on forward-scattered light were carried out on liver samples with a thickness similar to that of samples investigated previously.<sup>36</sup>

## 2. Materials and Methods

### A. Principle

To analyze the polarization of the transmitted light we measured the four Stokes parameters of the coherence matrix<sup>37</sup>:

$$\rho = \begin{bmatrix} \rho_{yy} & \rho_{xy} \\ \rho_{yx} & \rho_{xx} \end{bmatrix}.$$

The degree of polarization  $P$  is then given by the formula

$$P^2 = 1 - \frac{4(\rho_{xx}\rho_{yy} - |\rho_{xy}|^2)}{(\rho_{xx} + \rho_{yy})^2}.$$

For  $P = 1$  the light is fully polarized;  $P = 0$  means that the light is completely depolarized. This degree of polarization describes the transmitted polarization for a linear incident polarization. In practice, in the case of spherical scatterers it is often considered that the polarization contrast, directly computed from  $\rho_{yy}$  and  $\rho_{xx}$  only, can completely describe the state of polarization of the scattered light. For tissue samples, in which scatterers are not spherical, however, a more precise description using the degree of polarization should be considered when the nondiagonal components  $\rho_{yx}$  and  $\rho_{xy}$  are nonzero.

### B. Experimental Setup

The experimental setup is sketched in Fig. 1. A cw helium–neon laser polarized along the vertical ( $Oy$ ) direction was split at the input of a Mach-Zehnder-type interferometer. In one of the arms of the interferometer two acousto-optic modulators introduced

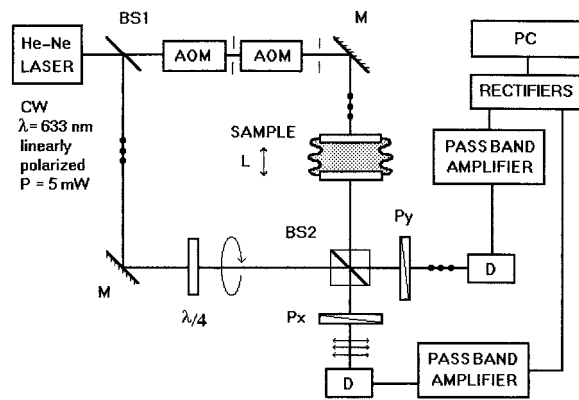


Fig. 2. Schematic diagram of the dual-channel interferometer for in-time polarization contrast measurement. PC, personal computer; BS1, beam splitter; BS2, polarization beam-splitting cube; Py, linear polarizer oriented vertically; Px, linear polarizer oriented horizontally; D's, P-I-N diode detectors; M's, mirrors;  $\lambda/4$ , quarter-wave plate; AOM's, acousto-optic modulators.

a frequency shift of 1.3 kHz upon the probe beam. This frequency shift yielded an oscillating signal upon the detector, and the contrast of this beating is recorded. We used the calibration routine described in detail in Ref. 30 to obtain the optical thickness that corresponds to  $\ln I/I_0$  for each sample thickness.

For additional experiments on liver samples we used the setup sketched in Fig. 2. This setup is less efficient than the previous one in rejecting the unwanted polarization in each channel because the beam splitter used after the sample cannot be optimized at the same time for alignment of the interferometer and for rejection of perpendicular polarizations, but it allowed us to measure simultaneously both parallel- and perpendicular-polarized components of the light emerging from the sample. In this case we achieved the calibration by inserting a half-wave plate at  $45^\circ$  and by replacing the sample by a series of calibrated neutral-density filters.

### C. Samples

Human blood was heparinized and diluted with isotonic saline solution. Calf liver was obtained from a butcher's shop, and slides were cut after freezing. Two parallel flat glass sheets held the sample at a given thickness owing to four calibrated wedges.

Suspensions of polystyrene ( $n = 1.588$ ) microspheres of diameters  $d = 200, 430, \text{ and } 940 \text{ nm}$  were used as an experimental model. Various concentrations were obtained by dilution in distilled water. To vary the sample thickness accurately from 0 to 14 mm we specially designed an adjustable cell with two glass plates and a micrometric screw. This cell permits perfect optical alignment to be maintained during both calibration and measurement. We achieved calibration by recording the detected voltage for a set of calibrated neutral-density filters inserted into the measurement arm of the interferometer.

### D. Calculations

Computing the degree of polarization from the coherence matrix requires four independent measurements of the Stokes parameters. To compute the whole coherence matrix we need to determine the nondiagonal components. Without any half-wave or quarter-wave plate in the signal arm after the diffusing sample, the heterodyne detection selects the parallel polarization  $\rho_{yy}$  of the intensity  $I$  of the transmitted light. The perpendicular component  $\rho_{xx}$  is measured by suitable rotation of a polarizer and a half-wave plate after the sample (Fig. 1). To measure the nondiagonal components ( $\rho_{xy}$  and  $\rho_{yx}$ ) of the coherence matrix we measured  $\rho_{ii} = 1/2(\rho_{yy} + \rho_{xx}) - \text{Re}(\rho_{xy})$  and  $\rho_{++} = 1/2(\rho_{yy} + \rho_{xx}) - \text{Im}(\rho_{yx})$ . To obtain  $\rho_{ii}$  we chose a polarizer and a half-wave plate to select the linear polarization at  $45^\circ$ . We obtained the values for  $\rho_{++}$  by introducing a quarter-wave plate behind the sample. The polarization degree calculated from the coherence matrix ranges theoretically from 1 (perfectly polarized) to 0 (fully depolarized). For extinction calculations we compared the amplitude of the heterodyne signal with the calibration curve. Results were obtained in terms of optical density (OD) and finally expressed in terms of optical thickness (OT) (as  $\text{OT} = \ln 10 \text{ OD}$ ). For the sake of clarity the four polarization states are not included in the figures that follow; but only  $\text{OT}_{yy}$ , which is the linear component parallel to the incident polarization, and  $\text{OT}_{xx}$ , which is the linear component perpendicular to the incident polarization, are shown.

Assuming a low density of microspheres, theoretical values of the scattering mean free path (SMFP)  $l_s$  are given by  $l_s = 1/N\sigma_s$ , where  $N$  is the number of particles per volume unit and  $\sigma_s$  is the scattering cross section of a scatterer.<sup>37,38</sup> The transport mean free path  $l'$  was calculated from the SMFP  $l_s$  because  $l' = l_s/(1 - g)$ , where the asymmetry factor  $g$  depends on the microsphere diameter and on the wavelength of light. Values of  $\sigma_s$  and  $g$  were computed from Mie theory.

Measuring the attenuation of the  $\text{OT}_{yy}$  component, we observed two regions with different slopes. The first slope, governed by the unscattered (ballistic) light component, follows the exponential law  $I = I_0 \exp(l_s^{-1}L)$ . The second slope, governed by the scattered (diffusive, snakelike) light component, seems to follow a different law. As our experiments did not allow us to discriminate between an exponential and a power-law dependence, we considered an exponential law for the sake of simplicity. Doing so allowed us to define a new scale,  $l_{\text{diff}}$ , by assuming that  $I = I_0 \exp(l_{\text{diff}}^{-1}L)$ . Fitting these slopes to the two different exponential functions allowed us to retrieve  $l_s$  and  $l_{\text{diff}}$ .

We also defined a new thickness  $L_{\text{scat}}$ , which is the limit from which the scattered component dominates the ballistic one. At this threshold the value  $\text{OT}_{\text{scat}} = L_{\text{scat}}/l_s$  corresponds to a mean number of SMFP's up to which ballistic transmission is still dominating. Recently we reported from a study with latex beads

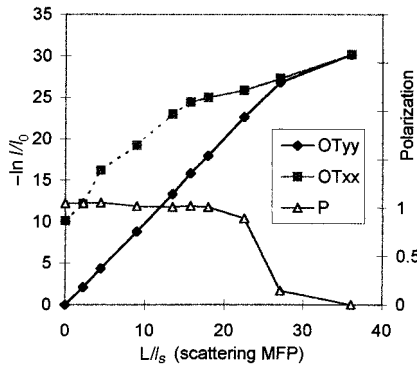


Fig. 3. Extinction corresponding to Stokes parameters:  $OT_{yy}$  parallel and  $OT_{xx}$  perpendicular with the incident polarization versus thickness for polystyrene microspheres of 200-nm diameter suspended in water at a number density of  $2.06 \times 10^9 \text{ mm}^{-3}$ . (For the sake of clarity,  $OT_{ii}$  linear at  $\pi/4$  and  $OT_{++}$  circular components are not plotted.)  $P$ , degree of polarization computed from the four Stokes parameters; MFP, mean free path.

that  $OT_{\text{scat}}$  depends weakly on the particle density but mainly on the particle diameter.<sup>35</sup> It is convenient to use this parameter to quantify the maximum thickness for direct imaging through a given scattering medium by use of only straightforward photons. Imaging through samples with large scatterers is hence restricted to lower OT than for samples with smaller scatterers. For samples with large scatters, such as tissues, the remaining polarization should provide a method for investigating the depth above the ballistic path, as we do here.

We previously demonstrated that the relative heterodyne efficiency  $\gamma'$  could provide an interesting parameter to quantify the wave-front degradation within a scattering medium.<sup>36</sup> Assuming that  $\gamma'$  does not depend on the medium thickness, i.e., that the law of attenuation of the scattering component is exponential, we can estimate the degradation by extrapolating the curve of the scattered component to  $L = 0$  [ $\gamma' = OT_{(0)}$ ]. This value might be useful for characterizing a scattering medium, mainly when  $l_s$  cannot be easily measured as in case of dense tissue.

### 3. Results

#### A. Experiments on Calibrated Suspensions of Polystyrene Beads

Figure 3 shows the light-extinction curves expressed in terms of OT and the corresponding depolarization degree as a function of the medium's thickness for polystyrene microspheres of 200-nm diameter at a density of  $2.06 \times 10^9$  particles  $\text{mm}^{-3}$ . The first part of the curve (from 0 to 26 SMFP's) corresponds to the exponential decay of the parallel polarized light ( $OT_{yy}$ ) and allows us to measure  $l_s = 0.22 \text{ mm}$  with a standard deviation of 6%. From this value we calculated a scattering cross section  $\sigma_s$  of  $2.19 \times 10^{-9} \text{ mm}^2$ , which is in good agreement with the value of  $2.4 \times 10^{-9} \text{ mm}^2$  calculated from Mie theory. Therefore this exponential decay is due to the attenuation of ballistic photons. As expected, the polarization of the transmitted light is

Table 1. Results Obtained for 200-nm Latex Microspheres ( $g = 0.32$ )<sup>a</sup>

$I_{s \text{ th}}$ (mm)	$I_{s \text{ mes}}$ (mm)	$I'$ (mm)	$I_{\text{diff}}$ (mm)	$L_{\text{scat}}$ (mm)	$OT_{\text{scat}}$	$OT_{(0)}$
0.081	0.106	0.119	1.376	2.5	23.7	22
0.202	0.237	0.297	—	>6	—	—
0.403	0.403	0.593	—	>10	—	—

<sup>a</sup>The measured SMFP  $L_{s \text{ mes}}$  is close to its theoretical value  $l_{s \text{ th}}$ . In this case the second component was observed only for the strongest particle number. For a thickness  $L = 0$  the linear extrapolation of the second component curve converges toward the  $OT_{(0)}$  value.

maintained in this regime. We carried out experiments with two other particle concentrations. The breakdown of parallel transmittance was observed close to the detectivity limit of our setup for the highest particle concentration investigated. The main results are gathered in Table 1.

For 430-nm polystyrene microspheres the first component of the light-extinction curve obeys the law of exponential decay as long as ballistic photons are dominant. A SMFP  $l_s$  was calculated from the slope of the three first points in Fig. 4 and of the ten first points in Fig. 5. For a theoretical scattering cross section of  $82 \times 10^{-9} \text{ mm}^2$ , results obtained from Figs. 4 and 5 lead to measured values of  $72 \times 10^{-9}$  and  $66 \times 10^{-9} \text{ mm}^2$ , respectively, after subtraction of the scattered component extrapolated from the second slope. Figure 4 shows a decrease of the degree of polarization for a thickness  $L_{\text{scat}}$  at which the light-extinction curve changes its slope dramatically. In other words, as expected, light depolarization occurs as soon as the scattering regime of propagation becomes dominant. For various particle concentrations this behavior appeared at a similar optical thickness, as illustrated in Fig. 5. In both cases (Figs. 4 and 5) the slope of the last five points allowed us to calculate the value of  $l_{\text{diff}}$ . Table 2 summarizes the results for various concentrations. The com-

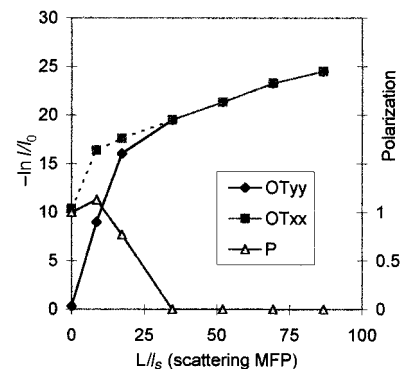


Fig. 4. Relationship between extinction of the polarization states and thickness for microsphere suspensions of 430 nm ( $N = 2.16 \times 10^8$  particles  $\text{mm}^{-3}$ ). The first part of the curve obeys the exponential law of ballistic propagation. The polarization degree decreases when the diffuse regime is observed.  $P$ , degree of polarization; MFP, mean free path.

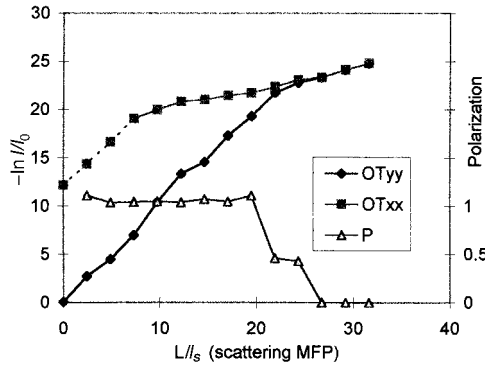


Fig. 5. Same polystyrene microspheres as in Fig. 4 but here with the suspension less concentrated ( $N = 2.7 \times 10^7$  particles  $\text{mm}^{-3}$ ). The diffuse regime is reached at a larger thickness.  $P$ , degree of polarization; MFP, mean free path.

puted values for  $OT_{\text{scat}}$  are of the order of 20 scattering events (see Table 2).

Figure 6 shows an example of extinction obtained for 940-nm polystyrene microspheres with  $N = 4.32 \times 10^6$   $\text{mm}^{-3}$ . For this diameter slightly greater than the wavelength, the degree of polarization decreases more slowly than in the case of small microspheres. The decrease in polarization goes from  $L_{\text{scat}} \approx 2$  mm (with  $L_{\text{scat}}/l_s = 15$  SMFP's) to a length

Table 2. Results Obtained for 430-nm Latex Microspheres ( $g = 0.77$ )<sup>a</sup>

$l_{s \text{ th}}$ (mm)	$l_{s \text{ mes}}$ (mm)	$l'$ (mm)	$l_{\text{diff}}$ (mm)	$L_{\text{scat}}$ (mm)	$OT_{\text{scat}}$	$OT_{(0)}$
0.056	0.068	0.244	0.718	1.31	19.4	16.3
0.112	0.138	0.488	1.024	2.79	20.2	16.6
0.225	0.261	0.977	1.194	5.67	21.7	16.9

<sup>a</sup>The threshold path length  $L_{\text{scat}}$  increases with dilution, but  $OT_{\text{scat}} = L_{\text{scat}}/l_{s \text{ mes}}$  depends weakly on the particle concentration. For  $L = 0$  the linear extrapolations of the second component curves converge toward  $OT_{(0)}$  values that are almost identical for the three concentrations tested.

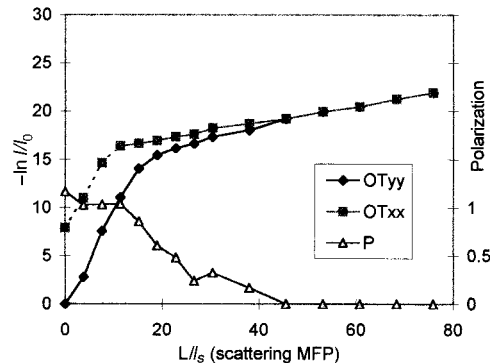


Fig. 6. Relationship between the extinction of polarization states and the medium's thickness for microsphere suspensions of 940 nm ( $N = 4.32 \times 10^6$  particles  $\text{mm}^{-3}$ ). The polarization is partially preserved for the lower part of the diffuse regime, which corresponds to the snake component.  $P$ , degree of polarization; MFP, mean free path.

Table 3. Results Obtained for 940-nm Latex Microspheres ( $g = 0.92$ )<sup>a</sup>

$l_{s \text{ th}}$ (mm)	$l_{s \text{ mes}}$ (mm)	$l'$ (mm)	$l_{\text{diff}}$ (mm)	$L_{\text{scat}}$ (mm)	$OT_{\text{scat}}$	$OT_{(0)}$
0.056	0.063	0.666	0.707	0.95	15.2	13.7
0.14	0.138	1.665	1.197	2.14	15.6	14
0.28	0.315	3.335	2.225	5.27	16.7	14.2

<sup>a</sup>The same conditions hold as for Table 2. The diffuse length  $l_{\text{diff}}$  that corresponds to the slope of the second component can be compared with the theoretical transport length  $l'$  computed from  $l_{s \text{ th}}/(1 - g)$ .

$L_{\text{diff}} \approx 6$  mm (first value where  $P = 0$ ), corresponding to  $L_{\text{diff}}/l_s = 48$  SMFP's. Even over  $L_{\text{diff}}$ , scattered photons are detected up to a maximum length  $L_{\text{max}} \approx 10$  mm (with  $L_{\text{max}}/l_s = 80$  SMFP's). The slope of the scattered component (calculated from the last eight points in Fig. 6) allows us to calculate a diffuse length  $l_{\text{diff}}$  that is almost ten times longer than  $l_s$ . Above  $L_{\text{diff}}$ , we assume that the detected signal is due to scattered light. The phase and the polarization of the transmitted light are perfectly random, corresponding to a degree of polarization  $P = 0$ . The main results for 940-nm bead suspensions are gathered in Table 3.

Because of signal fluctuations in the scattering regime, we plotted average OT and average polarization degree values. Figure 7 shows examples of the heterodyne signal at the intermediate frequency for three different path lengths. Figure 7(a) corresponds to ballistic propagation ( $L < L_{\text{scat}}$ ), where the signal amplitude is constant. By contrast, Figs. 7(b) and 7(c) correspond to the scattering regime ( $L_{\text{scat}} < L < L_{\text{diff}}$ ) and the diffusive regime ( $L_{\text{diff}} < L < L_{\text{max}}$ ), respectively, which exhibit large fluctuations.

## B. Experiments with Blood

To observe how polarized light behaves through a mammalian cell suspension we performed experiments on diluted human blood that permitted us to easily vary the sample thickness. Red blood cells are disks 7  $\mu\text{m}$  in diameter and  $\sim 2.5$   $\mu\text{m}$  thick; both dimensions are clearly greater than the wavelength. We carried out experiments on 1/5 and 1/10 diluted normal human blood, corresponding to cell concentrations of  $\sim 10^6$  and  $\sim 5 \times 10^5$   $\text{mm}^{-3}$  (volume fractions, 9% and 4.5%). We averaged the values given in Fig. 8 because of the large amplitude fluctuations. In this example  $l_s = 0.04$  mm was calculated from the slope of the three first points of the curve, which correspond to the ballistic component. This SMFP leads to a measured scattering cross section of  $50 \times 10^{-6}$   $\text{mm}^2$ , a reasonable value for a red cell whose larger section is  $\sim 38 \times 10^{-6}$   $\text{mm}^2$  and smaller section is  $18 \times 10^{-6}$   $\text{mm}^2$ . This value can be compared with the scattering cross section of  $64 \times 10^{-6}$   $\text{mm}^2$  measured with direct collimated detection.<sup>39</sup> Of course the polarization of the ballistic component remains parallel with the incident polarization. The threshold  $L_{\text{scat}}$  corresponds to 12.5 SMFP's. Similarly to the results obtained with large microspheres, the po-

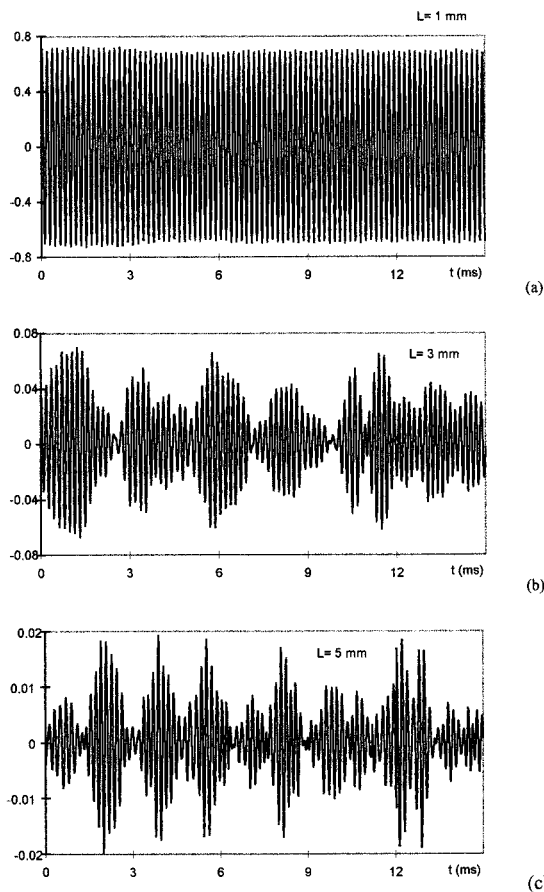


Fig. 7. (a) The amplitude of the heterodyne signal is constant for  $L = 1$  mm where ballistic propagation is dominant. (b), (c), Large fluctuations are typical of the scattered regime of propagation for  $L = 3$  and  $L = 5$  mm. Experience with latex beads of 940-nm diameter. Signal amplitudes are standardized. The time full scale is 15 ms. P, degree of polarization; MFP, mean free path.

polarization of the second component was partially preserved, decreasing progressively as the thickness increased to 11.2–12 mm (280–300 SMFP's).

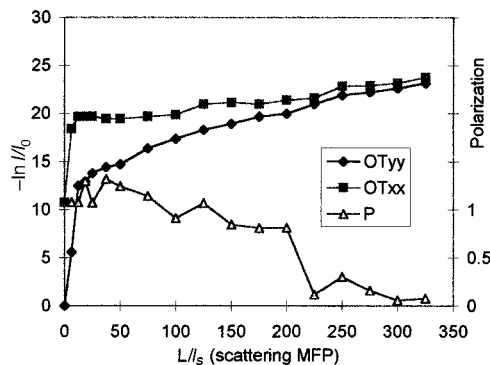


Fig. 8. Extinction of polarization states and polarization degree versus thickness for 1/5 diluted human blood. A polarized component continues for a few millimeters, even though the diffuse regime seems well established. Complete depolarization is obtained for larger path lengths when the signal vanishes at the detectivity limit of the method. P, degree of polarization; MFP, mean free path.

Table 4. Results Obtained for Diluted Human Blood<sup>a</sup>

$l_s$ mes (mm)	$l_{\text{diff}}$ (mm)	$L_{\text{scat}}$ (mm)	$OT_{\text{scat}}$	$OT_{(0)}$
0.016	0.761	0.196	12.5	13.7
0.04	1.31	0.5	12.5	13.8

<sup>a</sup>The same conditions hold as for Table 2. Blood hematocrits were 9 and 4.5 vol. %, respectively. In this case  $l_{\text{diff}}$  was  $\sim 40$  times longer than the measured SMFP.

Let us now consider the extinction coefficient in the scattering regime. For the 1/10 diluted blood sample, the diffuse length  $l_{\text{diff}}$  obtained from the slope of the second component was  $\sim 1.3$  mm, compared with  $l_s = 0.04$  mm for the ballistic component (Table 4). In the example shown in Fig. 8 for 1/10 diluted blood, the depolarization limit  $L_{\text{diff}}/l_s$  did not appear to be reached at 325 SMFP's. For 1/5 diluted blood (volume concentration, 9%) the value for  $l_{\text{diff}}$  is 0.76 mm, whereas  $L_{\text{diff}}/l_s$  does not exceed 280 SMFP's. This small behavioral difference could involve the role played by the particle concentration, the nonnegligible absorption that is due to hemoglobin in red cells, or both. It is noteworthy that extrapolation of the slope of the scattered component to  $L = 0$  gave  $OT_{(0)}$  values close to 13.8 SMFP's for both 4.5% and 9% blood-cell concentrations.

### C. Experiments on Tissue

In compact tissue a study of the detected light as a function of thickness is difficult to perform under reproducible conditions. With the setup shown in Fig. 1 the averaged polarization degree is close to 0; data acquisitions have a large uncertainty because polarized components are strongly fluctuating. Therefore we studied this phenomenon with the dual-channel polarized interferometer shown in Fig. 2. We achieved satisfactory measurements of thick liver slices (1–6 mm) that showed to a progressive depolarization of the transmitted light (Fig. 9). The slope of the scattered component within the 1–6-mm thickness range corresponds to a mean  $l_{\text{diff}} = 0.61$  mm ( $0.5 < l_{\text{diff}} < 0.83$ ;  $n = 5$ ), compared with 0.77 mm observed previously at the same wavelength.<sup>40</sup> Through a 1-mm sample, transmitted light remains

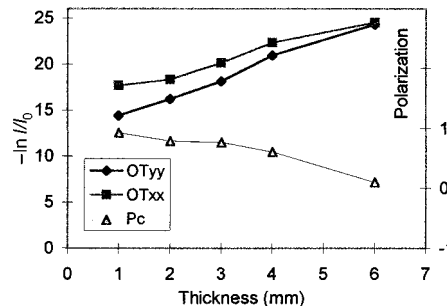


Fig. 9. Average values of polarized components  $OT_{yy}$  and  $OT_{xx}$  and average light polarization versus thickness for liver tissue. Pc, polarization contrast.

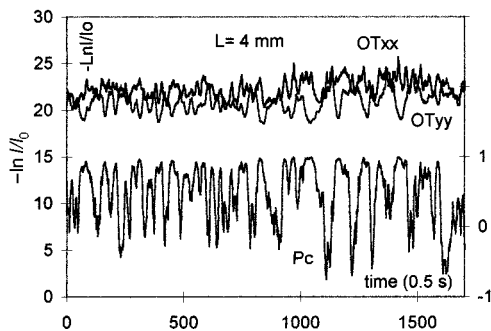


Fig. 10. Fluctuations of polarized components  $OT_{yy}$  and  $OT_{xx}$  and instantaneous polarization contrast  $Pc$  recorded during 5 min (2 points/s) in a 4-mm-thick liver sample.

polarized; the intensity of the parallel component always remains greater than the intensity of the perpendicular component, and these components fluctuate weakly. Through a 6-mm sample, however, the mean polarization is close to 0 but the instantaneous polarization strongly fluctuates from +1 to -1. Figure 10 shows fluctuations of the light attenuation in parallel ( $OT_{yy}$ ) and perpendicular ( $OT_{xx}$ ) directions and the polarization contrast  $Pc$  for an intermediate thickness at which polarized components are not randomized. We assume that, except for absorption and scattering, there is no significant optical activity in liver tissue. The time constant of fluctuations, which varies from a few seconds to 1 min, is larger in liver than in particle suspensions or blood.

In this experiment,  $OT_{scat}$  cannot be directly determined. In fact, this parameter should be close to  $OT_{(0)} = 13$ , which can be obtained by extrapolation of the curve on the  $OT$  axis for  $L = 0$ .

#### 4. Discussion

##### A. Experimental Errors

To achieve convenient measurements through liquid samples we specially designed an adjustable cell whose faces stay perfectly aligned during the whole experiment from  $L = 0$  to  $L = 14$  mm. Such a cell reduces errors that result from the misalignment of the optical axis. Moreover, calibration of the setup can be done through the cell for  $L = 0$  at any time during the experiment. To compute the attenuation that is due to polystyrene microspheres we neglected the absorption of water. Hence we observed good agreement between theoretical and experimental values for the ballistic component. The absorption of water may, however, influence the slope of the scattered component.<sup>41</sup>

Computing the degree of polarization depends on four independent measurements, which introduce more experimental errors than polarization contrast based on only two measurements. Errors were due mainly to large signal fluctuations during the acquisition time. Theoretically the polarization contrast is efficient for perfectly spherical particles such as polystyrene microspheres. However, it does not ap-

ply to nonspherical particles<sup>42</sup> such as blood cells or tissue such as muscle that exhibits asymmetric structures. In our series of polystyrene microspheres the values of polarization contrast appeared less dispersed and relatively close to the degree of polarization.

The polarizer that we used to select linear polarization provided maximal  $10^5$  extinction ( $OT = 11.5$ ) in the perpendicular direction. Therefore,  $OT_{xx}$  values were largely underestimated within the ballistic range of measurement. For this reason we plotted these underestimated  $OT_{xx}$  values with dotted curves in the figures above. Nevertheless, inaccuracies in the degree of polarization remain negligible in this range because the degree of polarization is close to 1. However, we verified with a double-sheet polarizer that the perpendicular polarization was actually cut off in the ballistic regime.

##### B. Signal Fluctuations

Because of the strong fluctuations in the scattered regime<sup>43</sup> we time averaged the signal over several tens of seconds for polystyrene microspheres and over  $\sim 1$  min for blood. We noted that fluctuations are stronger for the 940-nm microspheres than for the smaller ones. For blood samples the time constant of the fluctuations is longer than for polystyrene microspheres. We attribute these fluctuations to the Brownian motion of the scatterers in the aqueous suspension.<sup>44</sup> For the large microspheres and red blood cells the time constant of the motion is slow enough to permit the speckle pattern to be observed when the detector is replaced by a CCD camera. The smaller microspheres ( $d = 200$  nm) yield no visible speckle pattern because they move too fast relative to the integration time of the CCD camera, which time averages their speckle pattern. We verified this behavior by deliberately moving the larger scatterers ( $d = 940$  nm) by inducing a flow in the cell by pumping the suspension: The signal in the scattered regime disappeared. This result is in agreement with the assumption that the speckle pattern of the scatterers moves faster than the time constant of the heterodyne detection.<sup>45</sup> The time constant of the fluctuations is still longer in liver samples than in diluted blood. These fluctuations are similar to the speckle fluctuations observed when biological objects are illuminated with laser light.<sup>44</sup> In this case the displacement of scatterers should be slightly different from a pure Brownian motion.

There are also experimental errors that are due to signal fluctuations that provide uncertainties for low signals obtained with large particles or tissue. Therefore the actual limit of detectivity, i.e., the noise level, was somewhat underestimated for measurements with larger particles than with smaller ones.

##### C. Discussion of Results

We observed good agreement between the theoretical and the experimental values of  $l_s$  for latex beads as long as the ballistic component existed. The part of the concentration in the regime of propagation must

be separated from dependence on path length because it might influence the extinction coefficient, which does not depend exclusively on  $l_s$ .<sup>46,47</sup> According to Ishimaru,<sup>46</sup> the attenuation constant decreases when the particle concentration exceeds  $\sim 1\%$  in volume. This phenomenon is not in agreement with the exponential law of attenuation, because Mie theory applies to a medium in which particles are independent. Therefore, to apply the formula  $l_s = 1/N\sigma_s$  properly to the coherent extinction, we require a relatively low particle concentration, as in our experiments with latex suspensions. Of course, this hypothesis will hardly be credible with actual mammalian tissues.

The use of a low-coherence pulsed source to characterize the scattered component was described by Hee *et al.*<sup>17,18</sup> Using a different method based on a superluminescent diode, Chan *et al.* recently reported similar results with an Intralipid fat emulsion.<sup>48</sup> Our results are in agreement with experiments reported in that paper in which the scattered light obtained with a light source with a long coherence length is rejected by a low-coherence diode. The present research has yielded additional information on the state of polarization of scattered light as a function of the medium's thickness and relates it to particle size or volume fraction. Both concentration and path length influence the number of scattering events. In fact, the weak slope of the scattered component in our experiments is due not to an increased concentration but to a larger path length.

It is noteworthy that the measured diffuse length can be compared with the theoretical value of the transport length  $l' = l_s/(1 - g)$  calculated from  $l_s$  and the asymmetry factor  $g$  obtained from Mie theory for each particle diameter. For 200-nm beads the inaccuracy in  $l_{\text{diff}}$  measurements precludes any practical comparison. For 430-nm particles, which yield theoretical  $l'$  values four times larger than the SMFP, measured  $l_{\text{diff}}$  values are clearly greater than the theoretical  $l'$  values (see Table 2). For 940-nm particles the theoretical transport length exceeds ten times the SMFP (see Table 3) and is of the order of  $l_{\text{diff}}$ . Further experiments will be necessary to determine the factors that influence the slope of the scattered component; for example, the absorption coefficient might play a part that we did not study here.

Comparison of our results with data already published is limited because in most of the latter the measurements were made with a fixed sample thickness. Despite methodological differences, our results with polystyrene beads are in agreement with those of the time-resolved experiments of Demos and Alfano with 1070-nm polystyrene suspensions, thus demonstrating that the early photons of the scattered component (snakelike photons) retain part of the initial polarization before complete depolarization.<sup>21</sup>

Our results on the depolarization of light with latex spheres can be compared with results obtained by Bicout *et al.*<sup>30,34</sup> They theoretically and experimentally studied the depolarization of light after it passed through a scattering medium. In their study the

size parameter  $ka$  (where  $a$  is the radius of particles and  $k$  is the wave number) was 5.89 in the Mie region of propagation, 2.69 in the intermediate region, and 1.23 in the Rayleigh region. In our experiments the size parameters are 4.66, 2.15, and 1, respectively. In the Rayleigh region, we observed that linearly polarized light disappears after 30 SMFP's, whereas Bicout *et al.* found only 15 SMFP's. For the intermediate size parameter, depolarization was achieved after 27–35 SMFP's in our experiment, close to the 25 SMFP's found by Bicout *et al.* In the Mie region we observed that light is depolarized after 50 SMFP's; 65 SMFP's are reported by Bicout *et al.* The differences could be due to the particle concentration. At any rate, the two measurements of the part of the particle diameter in the depolarization of light are in agreement.

In spite of the differences in structure and concentration between large polystyrene particles and blood, the intermediate scattering regime of light propagation appears similar. In contrast to small latex beads, blood degrades progressively in the coherent regime, where initial direction and polarization are gradually lost before a purely diffuse incoherent regime results. Our study required  $\sim 280$  scattering events to depolarize light through a red blood cell suspension, which confirms the influence of the particle diameter that enhances the scattering (polarization) length.

The influence of the particle diameter on the fringe pattern of backscattered light was reported for both polystyrene and mammalian cell suspensions.<sup>49</sup> Unfortunately, a direct comparison with our results cannot be made because the on-axis and low-order modes were suppressed to reject the strong specular reflection from the surface at the laser input point. At any rate, it has been envisaged that depolarization of light is quite different in the backward and the forward directions.<sup>33</sup> Inasmuch as we know how the diameter influences the depolarization, the main question to answer actually concerns the nature of the scatterer that interferes with light in dense biological tissues.

The coherence degradation is more difficult to analyze for liver tissue than for particle suspensions because  $l_s$  is short in the former case. It cannot be enhanced by dilution as with blood. We found experimental values for  $l_s$  in mammalian liver measured with another method available in the literature: 0.032 mm (Marchesini *et al.*<sup>50</sup>) and 0.069 mm (Parsa *et al.*<sup>51</sup>). Assuming that depolarization is almost complete for  $L = 6$  mm, the number of scattering events necessary to reach this state is 188 or 87, depending on the value of  $l_s$ . Because the scattered component characterized by our method yields  $l' = 0.61$  mm, we can also estimate the number of transport lengths that randomizes the linear polarization to be approximately 10. We are not surprised that polarization is preserved for a few millimeters through liver tissue because light echoes in mammalian tissues at depths of as much as

1.5 mm have been obtained by low-coherence reflectometry.<sup>52</sup>

It is noteworthy that the second component can be extrapolated at  $OT_{(0)} = 13.8$  for blood cells and  $OT_{(0)} = 13$  for liver tissue. Assuming that the  $OT_{scat}$  threshold is related to the particle diameter, we wonder whether the interacting structure in liver tissue is the liver cell itself (which has an approximate size of 25–30  $\mu\text{m}$ ) or its nucleon (whose diameter of 7  $\mu\text{m}$  is close to that of a red blood cell). According to Beauvoit *et al.*, the main scattering particles in liver are mitochondria, which are submicrometric intracellular organelles.<sup>53</sup> This finding would support those in the recent study of cell suspensions made by Hielscher *et al.*<sup>49</sup> On the contrary, the validation of a model of a fractal distribution of sizes of scattering centers in tissues ranging from a few nanometers to several micrometers<sup>54</sup> would suggest that mammalian tissue can actually appear as a heterogeneous structure in which refractive-index inhomogeneities are not necessarily superimposed upon the histologic structure of the tissue.<sup>55</sup>

#### D. Discussion of the Hypothesis

Our experiments test two coherence criteria simultaneously, because heterodyne detection requires wave-front matching between signal and reference waves. The first criterion is related to the efficiency of the optical heterodyne detection, which decreases in the scattering regime because of wave-front degradation. The second criterion is the degree of polarization, which remains unchanged in the ballistic regime because of the coherent reconstruction in the forward direction. In the ballistic regime, from  $L = 0$  to  $L_{scat}$ , the degree of polarization remains close to 1. In the scattering regime from  $L_{scat}$  to  $L_{diff}$  the degree of polarization remains above 0, decreasing progressively as a function of thickness. We have already mentioned that the normalized length  $L_{scat}/l_s$  ( $=OT_{scat}$ ) is a good criterion to use to locate the beginning of the scattered component in suspensions because it depends weakly on the particle density for a given particle size. After  $L_{diff}$ , the initial polarization was lost. Inasmuch as  $OT_{scat}$  depends weakly on the particle concentration, it is convenient to use this value to characterize the limit of direct imaging when the scattered light blurs the image. By contrast, the limit of the diffuse imaging based on the polarization can reach  $L_{diff}$ , which is much greater than  $L_{scat}$  in tissues.

The particular regime of scattered propagation characterized by breakdown of the attenuation coefficient and large signal fluctuations was weakly influenced by particle concentration (Tables 1–4). The main factor that influences the scattering threshold, i.e., degrades the coherent propagation, is the particle diameter, which governs the asymmetry factor. To explain this phenomenon we assume that wave-front degradation is easier to obtain in case of large particles. From this point of view, light in mammalian tissues behaves as in large particle suspensions.

For mammalian tissues our results on the polarization states do not appear different from those obtained by Demos *et al.* with a time-resolved detection method.<sup>56</sup> In our experiments the light polarization was progressively looser through thick tissue when coherently detected optical signals were time averaged. By contrast, instantaneous analysis of both polarized components showed that the degree of polarization undergoes large fluctuations. The time constant of fluctuations is long compared with to the heterodyne frequency. Therefore various zigzag modes that pass through the tissue with the same delay (or phase) can beat on the detector with the reference beam because we used a long coherence laser source. To better understand how light propagates in mammalian tissues, we intend to perform additional analysis of the polarization in tissues by using a low-coherence source. The preservation of the light polarization should not be the coherence criterion for detecting informative photons because Devaraj *et al.* recently reported using a long-coherence laser source to produce anatomical images of the human finger.<sup>29</sup>

The most important result that we must consider is the huge increase of the transport length in the scattering regime that lasts for ten times the SMFP for 940-nm latex beads and even 50 times the path for blood cell suspensions or tissues. Such data lead us to expect that optical diffuse tomography based on a coherent detection method can be efficiently applied to investigate tissue or organs at least 10 mm thick.

#### 5. Conclusion

In our experiments on particle suspensions we studied the degree of polarization as a function of sample thickness. We examined both polarization and coherence degradation from the ballistic component (coherent) up to the limit where the whole light became purely diffuse (incoherent). The polarization of the emerging light began to decrease at the optical thickness where the scattered component began to appear, whereas the scattering threshold strongly depended on the particle diameter. The possibility to vary the sample thickness continuously for a given medium allowed us to identify accurately the characteristics of the scattered component detected coherently: increased transport length compared with the scattering mean path, decrease of the degree of polarization, and large fluctuations influenced by Brownian motion and stirring of the medium.

Experiments on calibrated latex bead suspensions clarified the influence of particle diameter on the degradation of the coherent field. The number of scattering events necessary to degrade the ballistic propagation decreased when the particle diameter increased. By contrast, the transport length of the scattered polarized component increased with the particle diameter.

As it passed through scattering mammalian tissues, the scattered component of coherently detected light partly maintained its initial polarization for a few millimeters, even though the ballistic component

became too weak to be detected. Between the pure ballistic regime of propagation limited to some hundreds of micrometers in tissue and the pure diffuse regime where photons polarization and phase are perfectly random, scattered photons propagated for several millimeters, exhibiting partial memory of their initial direction, polarization, and coherence. A significant amount of these scattered photons was detected by the optical heterodyne detection method. Thus investigations in deeper tissue samples should be possible by this method than by use of purely collimated photons.

The authors are grateful to Bernard Gélébart and Thierry Lépine for computing the scattering cross section and the asymmetry factor of the polystyrene microspheres used in this research. The authors thank Florence Henry, who provided valuable assistance in the experimental measurements. This research is supported in part by the Institut National de la Santé et de la Recherche Médicale and by the Université Paris XII.

## References

1. E. N. Carlsen, "Transillumination light scanning," *Diagnostic Imaging* **3**, 28–33 (1982).
2. G. Jarry, S. Ghesquière, J.-M. Maarek, F. Fraysse, S. Debray, B.-M. Hung, and D. Laurent, "Imaging mammalian tissues and organs using laser collimated transillumination," *J. Biomed. Eng.* **6**, 70–73 (1984).
3. Y. Yamashita, S. Susuki, S. Miyaki, and T. Hayakawa, "The neonate brain (NIR) and breast imaging using transillumination," in *Photon Migration in Tissues*, B. Chance, ed. (Plenum, New York, 1988), Chap. 6, pp. 55–67.
4. J.-L. Martin, Y. Lecarpentier, A. Antonetti, and G. Grillon, "Picosecond laser stereometry light scattering measurement on biological materials," *Med. Biol. Eng. Comput.* **18**, 250–252 (1980).
5. S. Andersson-Engels, R. Berg, S. Svanberg, and O. Jarlman, "Time-resolved transillumination for medical diagnostics," *Opt. Lett.* **15**, 1179–1181 (1990).
6. B. B. Das, K. M. Yoo, and R. R. Alfano, "Ultrafast time gated imaging in thick tissues: a step toward optical mammography," *Opt. Lett.* **18**, 1092–1094 (1993).
7. A. D. Sappey, "Optical imaging through turbid media with a degenerated four-wave mixing correlation time gate," *Appl. Opt.* **33**, 8346–8354 (1994).
8. A. F. Fercher, K. Mengedoh, and W. Werner, "Eye length measurement by interferometry with partially coherent light," *Opt. Lett.* **13**, 186–189 (1988).
9. D. Huang, E. Swanson, C. Lin, J. Schuman, W. Stinson, W. Chang, M. Hee, T. Flotte, K. Gregory, C. Puliafito, and J. Fujimoto, "Optical coherence tomography," *Science* **254**, 1178–1181 (1991).
10. J. M. Schmitt, M. J. Yadlowsky, and R. F. Bonner, "Subsurface imaging of living skin with optical coherence microscopy," *Dermatology* **191**, 93–98 (1995).
11. M. Kempe and W. Rudolph, "Scanning microscopy through thick layers based on linear correlation," *Opt. Lett.* **19**, 1919–1921 (1994).
12. B. Bouma, G. J. Tearney, S. A. Boppart, M. R. Hee, M. E. Brezinski, and J. G. Fujimoto, "High-resolution optical coherence tomographic imaging using a mode-locked Ti:Al<sub>2</sub>O<sub>3</sub> laser source," *Opt. Lett.* **20**, 1486–1488 (1995).
13. B. Bouma, G. J. Tearney, I. P. Bilinsky, B. Golubovic, and J. G. Fujimoto, "Self-phase-modulated Kerr-lens mode-locked Cr:forsterite laser source for optical coherence tomography," *Opt. Lett.* **21**, 1839–1841 (1996).
14. J. M. Schmitt, A. H. Gandjbakhche, and R. F. Bonner, "Use of polarized light to discriminate short-path photons in a multiply scattering medium," *Appl. Opt.* **31**, 6535–6546 (1992).
15. H. Horinaka, K. Hashimoto, K. Wada, Y. Cho, and M. Osawa, "Extraction of quasi-straightforward-propagating photons from diffused light transmitting through a scattering medium by polarization modulation," *Opt. Lett.* **20**, 1501–1503 (1995).
16. O. Emile, F. Bretenaker, and A. Le Floch, "Rotating polarization imaging in turbid media," *Opt. Lett.* **21**, 1706–1708 (1996).
17. M. Hee, J. Izatt, E. Swanson, and J. Fujimoto, "Femtosecond transillumination tomography in thick tissues," *Opt. Lett.* **18**, 1107–1109 (1993).
18. M. Hee, J. Izatt, J. Jacobson, J. Fujimoto, and E. Swanson, "Femtosecond transillumination optical coherence tomography," *Opt. Lett.* **18**, 950–952 (1993).
19. M. J. Yadlowsky, J. M. Schmitt, and R. F. Bonner, "Multiple scattering in multiple coherence microscopy," *Appl. Opt.* **34**, 5699–5707 (1995).
20. S. P. Morgan, M. P. Khong, and M. Somekh, "Effects of polarization state and scatterer concentration on optical imaging through scattering media," *Appl. Opt.* **36**, 1560–1565 (1997).
21. S. G. Demos and R. R. Alfano, "Temporal gating in highly scattering media by the degree of optical polarization," *Opt. Lett.* **21**, 161–163 (1996).
22. F. F. Jobsis, "Non-invasive infrared monitoring of cerebral and myocardial oxygen sufficiency and circulation parameters," *Science* **198**, 1264–1267 (1977).
23. G. Jarry, S. Debray, J. Perez, J. P. Lefebvre, M. de Filquelmont, and A. Gaston, "In vivo transillumination using near infrared laser pulses and differential spectroscopy," *J. Biomed. Eng.* **11**, 293–299 (1989).
24. A. E. Profio and G. A. Navarro, "Scientific basis of breast diaphanography," *Med. Phys.* **16**, 60–65 (1989).
25. S. Flock, B. Wilson, and M. Patterson, "Total attenuation coefficients and scattering phase functions of tissues and phantom material at 633 nm," *Med. Phys.* **14**, 835–841 (1987).
26. J.-P. Lefebvre, G. Jarry, and C. Jorand, "Optical processing of images obtained by transillumination of heterogeneous scattering and absorbing media," in *Optical Pattern Recognition II*, H. J. Caulfield, ed., *Proc. SPIE* **1134**, 154–159 (1989).
27. Q. Z. Wang, X. Liang, L. Wang, P. P. Ho, and R. R. Alfano, "Fourier spatial filter acts as a temporal gate for light propagating through a turbid medium," *Opt. Lett.* **20**, 1498–1500 (1995).
28. X. D. Li, T. Durduran, A. G. Yodh, B. Chance, and D. N. Pattanayak, "Diffraction tomography for biochemical imaging with diffuse-photon density waves," *Opt. Lett.* **22**, 573–575 (1997).
29. B. Devaraj, M. Usa, K. P. Chan, T. Akatsuka, and H. Inaba, "Recent advances in coherent detection imaging (CDI) in biomedicine: laser tomography of human tissues *in vivo* and *in vitro*," *IEEE J. Sel. Top. Quantum Electron.* **2**, 1008–1016 (1996).
30. D. Bicout, C. Brosseau, A. S. Martinez, and J. M. Schmitt, "Depolarization of multiple scattered waves by spherical diffusers: influence of size parameter," *Phys. Rev. E* **49**, 1767–1770 (1994).
31. F. C. MacKintosh, J. X. Zhu, D. J. Pine, and D. A. Weitz, "Polarization memory of multiply scattered light," *Phys. Rev. B* **40**, 9342–9345 (1989).

32. F. C. MacKintosh and S. John, "Diffusing-wave spectroscopy and multiple scattering of light in correlated random media," *Phys. Rev. B* **40**, 2383–2406 (1989).
33. R. L.-T. Cheung and A. Ishimaru, "Transmission, backscattering, and depolarization of waves in randomly distributed spherical particles," *Appl. Opt.* **21**, 3792–3798 (1982).
34. D. Bicout and C. Brosseau, "Multiply scattered waves through a spatially random medium: entropy production and depolarization," *J. Phys. (France) I* **2**, 2047–2043 (1992).
35. G. Jarry, E. Steimer, V. Damaschini, M. Jurczak, and R. Kaiser, "Coherent components of forward light propagation through scattering media," *J. Opt. (Paris)* **28**, 83–89 (1997).
36. G. Jarry, L. Poupinet, J. Watson, and T. Lépine, "Extinction measurements in diffusing mammalian tissue with heterodyne detection and a titanium-sapphire laser," *Appl. Opt.* **34**, 2045–2054 (1995).
37. A. Ishimaru, *Propagation and Scattering of Radiation in Random Media* (Academic, New York, 1978).
38. H. C. van de Hulst, *Light Scattering by Small Particles* (Wiley, New York, 1957).
39. J. M. Steinke and A. P. Shepherd, "Comparison of Mie theory and the light scattering of red blood cells," *Appl. Opt.* **27**, 4027–4033 (1988).
40. G. Jarry and L. Poupinet, "Heterodyne detection for measuring extinction coefficient in mammalian tissue," *J. Opt. (Paris)* **24**, 279–285 (1993).
41. B. Van Tiggelen, Laboratoire d'Expérimentation Numérique, Université Joseph Fourier, 38042 Grenoble, France (personal communication, 1997).
42. M. I. Mishchenko and J. W. Hovenier, "Depolarization of light backscattered by randomly oriented nonspherical particles," *Opt. Lett.* **20**, 1356–1358 (1995).
43. I. Freund, "Optical intensity fluctuations in multiply scattering media," *Opt. Commun.* **81**, 251–258 (1991).
44. J. D. Briers, "Speckle fluctuations and biomedical optics: implications and applications," *Opt. Eng.* **32**, 277–283 (1993).
45. E. Leith, P. Naulleau, and D. Dilworth, "Ensemble-averaged imaging through highly scattering media," *Opt. Lett.* **21**, 1691–1693 (1996).
46. A. Ishimaru and Y. Kuga, "Attenuation constant of a coherent field in a dense distribution of particles," *J. Opt. Soc. Am.* **72**, 1317–1329 (1982).
47. H. J. Schnorrenberg, M. Hengstebeck, and K. Schlinkmeier, "The attenuation of a coherent field by scattering," *Opt. Commun.* **117**, 541–549 (1995).
48. K. P. Chan, M. Yamada, and H. Inaba, "Coherence gating in optical heterodyne detection measurements of scattering and absorption in highly scattering media," *Appl. Phys. B* **63**, 249–253 (1996).
49. A. H. Hielscher, J. R. Mourant and I. J. Bigio, "Influence of particle size and concentration on the diffuse backscattering of polarized light from tissue phantoms and biological cell suspensions," *Appl. Opt.* **36**, 125–135 (1997).
50. R. Marchesini, A. Bertoni, S. Andreola, E. Melloni, and A. Sichirollo, "Extinction and absorption coefficients and scattering phase functions of human tissues *in vitro*," *Appl. Opt.* **28**, 2318–2324 (1989).
51. P. Parsa, S. L. Jacques, and N. S. Nishioka, "Optical properties of rat liver between 350 and 2200 nm," *Appl. Opt.* **28**, 2325–2330 (1989).
52. S. Boppart, B. Bouma, C. Pitris, G. Tearney, J. Fujimoto, and M. Brezinski, "Forward-imaging instruments for optical coherence tomography," *Opt. Lett.* **22**, 1618–1620 (1997).
53. B. Beauvoit, T. Kitai, and B. Chance, "Contribution of the mitochondrial compartment to the optical properties of the rat liver: a theoretical and practical approach," *Biophys. J.* **67**, 2501–2510 (1994).
54. B. Gelebart, E. Tinetti, J. M. Tualle, and S. Avriplier, "Phase function simulation in tissue phantoms: a fractal approach," *Pure Appl. Opt.* **5**, 377–388 (1996).
55. J. M. Schmitt and G. Kumar, "Turbulent nature of the refractive-index variations in biological tissue," *Opt. Lett.* **21**, 1310–1312 (1996).
56. S. G. Demos, H. Savage, A. S. Heerdt, S. Shantz, and R. R. Alfano, "Polarization preservation gate—a tool for optical mammography," in *Conference on Lasers and Electro-Optics*, Vol. 9 of 1996 OSA Technical Digest Series (Optical Society of America, Washington, D.C., 1996), paper CMD2, p. 20.